*on the Physics and Chemistry of Fission, Salzburg, Austria, 1965* (International Atomic Energy Agency, Vienna, Austria, 1965), p. 385.
[56]W. John, F. W. Guy, and J. J. Wesolowski, University of California Lawrence Radiation Laboratory Report No. UCRL-72501, also Phys. Rev. C 2, 1451 (1970).
[57]L. E. Glendenin and H. C. Griffin, Phys. Letters 15, 153 (1965).
[58]R. S. Hager and E. C. Seltzer, Nucl. Data A4, 1 (1968).
[59]C. D. Coryell, Ann. Rev. Nucl. Sci. 2, 304 (1953).
[60]J. Terrell, Phys. Rev. 108, 783 (1957). The photon energy release derivable from the method of this paper is given explicitly in Ref. 21.
[61]A. W. Cameron, Can. J. Phys. 35, 1021 (1957).
[62]P. A. Seeger, Nucl. Phys. 25, 1 (1961).
[63]I. Dostrovsky, Z. Fraenkel, and G. Friedlander, Phys. Rev. 116, 683 (1959).
[64]J. R. Grover and T. D. Thomas, in American Chemical Society Symposium on Recent Advances in Nuclear Science and Engineering Education, March 1966, Pittsburgh, Pennsylvania (unpublished); also J. R. Grover, private communication. This work gave additional results from the effort reported in Ref. 23.
[65]For example, Seeger (Ref. 62) reported that his mass formula gives a 0.75-MeV standard deviation with the input odd-$A$ masses, and his paper shows a systematic ~1-MeV error near mass 100. Initial fission fragments are away from the valley of $\beta$-ray stability, so lacking a published assessment of extrapolation uncertainties, one might expect systematic errors $\gtrsim$1 MeV/fragment in estimated initial excitation energy.

PHYSICAL REVIEW C VOLUME 3, NUMBER 1 1971

# Energy Levels in $Cf^{251}$ via Alpha Decay of $Fm^{255}$†

I. Ahmad, F. T. Porter, M. S. Freedman, R. F. Barnes, R. K. Sjoblom, F. Wagner, Jr., J. Milsted, and P. R. Fields

*Chemistry Division, Argonne National Laboratory, Argonne, Illinois 60439*

(Received 18 August 1970)

The $\gamma$-singles and conversion-electron spectra of $Fm^{255}$ were measured with a Ge(Li) diode and the Argonne double toroidal $\beta$-ray spectrometer, respectively. In the $\gamma$-ray spectra, in addition to the transitions expected from previously known decay schemes, $\gamma$ rays of energies 63.8, 131.0, 204.1, and 264.1 keV were observed. Two new $\alpha$ groups, $\alpha_{368}$ (6.765 MeV) and $\alpha_{433}$ (6.701 MeV), were identified in coincidence with 131.0- and 204.1-keV $\gamma$ rays. A two-parameter $\gamma$-$\gamma$ coincidence experiment showed that the 204.1- and 131.0-keV transitions populate the $\frac{9}{2}$ and $\frac{11}{2}$ members of the favored band. Conversion-electron studies and $\alpha$-vs-$\gamma$ intensity comparisons demonstrate their $E1$ character. The half-life of the 370.4-keV level was measured by a delayed $\alpha$-$\gamma$ coincidence method and found to be 1.3 ± 0.1 $\mu$sec. On the basis of these observations and the $\alpha$ intensities to these levels, the 370.4- and 434.2-keV levels have been assigned to the $\frac{11}{2}$−(725↑) and $\frac{9}{2}$ −(734↑) Nilsson states, respectively. A three-parameter $\alpha$-$\gamma$-time coincidence experiment indicates that the $\alpha$ intensity to the 105.73-keV ($I=\frac{7}{2}$, $K=\frac{1}{2}$) level is less than 1%, implying that its 18% population comes primarily via a 0.57-keV transition from the 106.30-keV, $I=\frac{7}{2}$, $K=\frac{7}{2}$ level. The $\alpha$ transition probabilities to various bands are in agreement with the values expected from $\alpha$-decay systematics and theoretical calculations. The $K$-, $L$-, $M$-, and $N$-sunshell atomic electron binding energies in Cf ($Z=98$), obtained experimentally by least-squares adjustment from the conversion-line data, show significant deviations below recent (Bearden and Burr) tabulated values.

## I. INTRODUCTION

The decay scheme of $Fm^{255}$ was first investigated by Asaro, Bjørnholm, and Perlman (ABP).[1] The ground state and the level at 106 keV in $Cf^{251}$ were given the Nilsson-state[2] assignments of $\frac{1}{2}$+(620↑) and $\frac{7}{2}$+(613↑), respectively. These assignments are based on the observed rotational level spacings, intensity patterns, and the multipolarities of prominent interband transitions. $\gamma$-$\alpha$ and electron-$\alpha$ coincidence measurements showed the existence of another level at 546 keV ($\alpha$ intensity = 0.05%) which decays via a 426-keV level to the 106-keV state. The 426- and 546-keV levels were given the tentative assignments of $\frac{9}{2}$+(615↓) and $\frac{11}{2}$−(725↑), respectively. Later work by Ahmad[3] showed that the $\alpha$ spectrum measured in coincidence with $\gamma$ rays is very complex, and the above assignments of the 426- and 546-keV levels are not correct. From his coincidence measurements, he was able to identify two new rotational bands with band-head energies at 178 and 550 keV, and assigned them to the $\frac{3}{2}$+(622↓) and $\frac{5}{2}$+(622↑) neutron states, respectively. A decay scheme representing a composite of the results obtained by ABP and Ahmad[3] is shown in Fig. 1. A recent study[4] of the electron

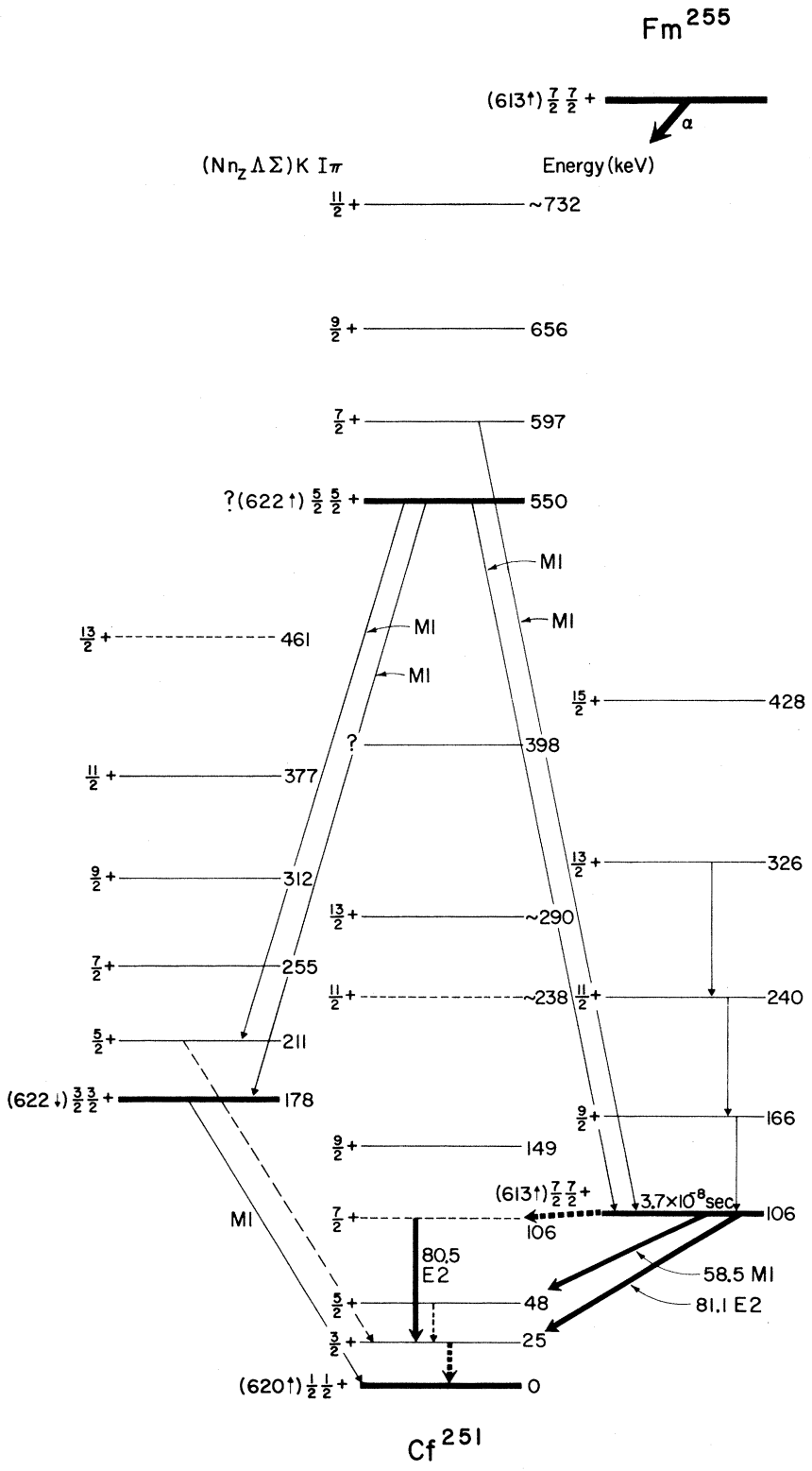


FIG. 1. Energy-level diagram of $Cf^{251}$ proposed in Refs. 1 and 2. The energies and assignments of states for $\frac{1}{2}^+$ and $\frac{7}{2}^+$ bands are taken from Ref. 1 and the energies and assignments of states for the $\frac{3}{2}^+$ and $\frac{5}{2}^+$ bands are taken from Ref. 2.

capture decay of $Es^{251}$ confirms the assignment of the 178-keV state.

Because of its high specific activity, $Fm^{255}$ is a very suitable source for the investigation of weakly populated states in $Cf^{251}$. From the Nilsson diagram[2] and the known states[5,6] in $Cf^{249}$ and $Cf^{253}$, several single-particle states are expected to lie ~400 keV above the ground state of $Cf^{251}$. Recently a large amount of $Fm^{255}$ has become available from the United States Atomic Energy Commission, and hence a detailed investigation of levels in $Cf^{251}$ was undertaken. The use of a high-resolution Ge(Li) diode, a high-resolution $\beta$-ray spectrometer, and a multiparameter analyzer enabled us to identify new single-particle states and confirm the assignments of previously known levels.

## II. SOURCE PREPARATION

Approximately 20 $\mu$g of Es containing ~0.05% $Es^{255}$ ($t_{1/2}$ = 39.8 day) was obtained from Oak Ridge National Laboratory as a part of the heavy-element production program. The $\beta^-$-decay daughter, $Fm^{255}$ ($t_{1/2}$ = 20.1 h), was chemically isolated several times and used for the present investigation. The Fm was first separated from Es and other actinides by adsorption on a cation-exchange resin column, followed by elution with ammonium $\alpha$-hydroxy isobutyrate.[7] The Fm was then purified from fission products by an extraction chromatographic procedure.[8] The sample was once again purified with a cation-exchange resin column[7] to remove any Es left over from the initial separation. For $\gamma$-ray spectroscopy the sample was spread on a thin glass plate with tetraethylene glycol and evaporated to dryness. The sources for $\alpha$ spectroscopy and $e^-$ spectroscopy were prepared by vacuum volatilization of the purified Fm onto thin Al foils.

## III. EXPERIMENTAL DATA

### A. $\alpha$ Spectroscopy

The $\alpha$-particle spectra of $Fm^{255}$ were measured with a 6-mm-diam Au-Si surface-barrier detector. Figure 2 shows an $\alpha$ spectrum measured at a low geometry (~0.2% of $4\pi$). The energies of the $\alpha$ groups were measured with respect to that of $Es^{253}$ $\alpha_0$ group which was taken as 6.632 MeV.[9]

A two-parameter $\gamma$-$\alpha$ coincidence experiment, which is discussed in more detail in Sec. III D, was performed to identify weak $\alpha$ groups. The $\alpha$ particles were detected with the same 6-mm-diam detector and the $\gamma$ rays were detected with a 25-$cm^3$ Ge(Li) diode. Two of the $\alpha$ spectra measured in coincidence ($2\tau$ = 2 $\mu$sec) with selected $\gamma$ rays are shown in Fig. 3. It should be noted that the

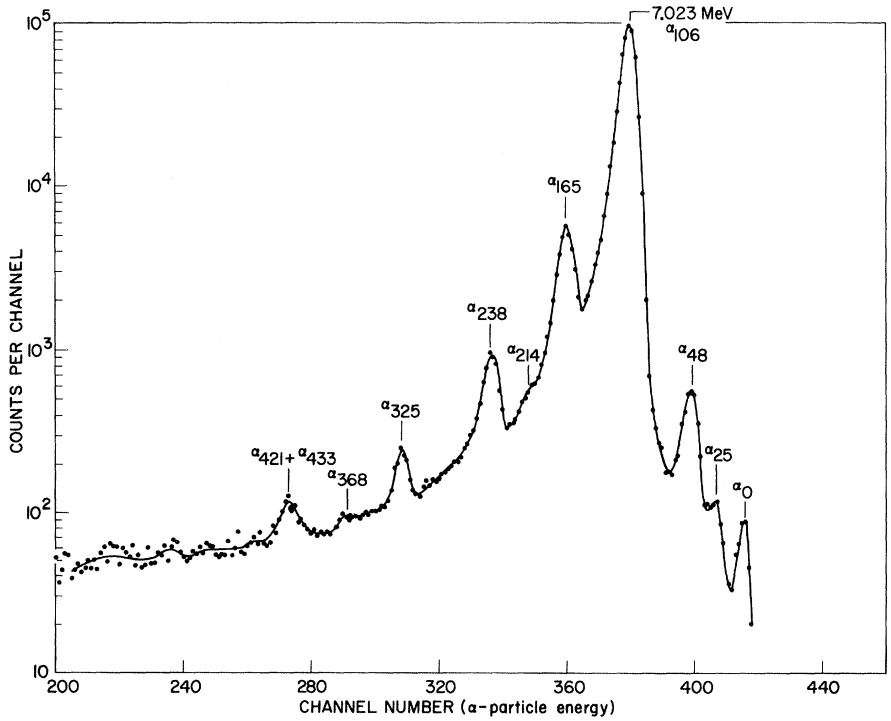


FIG. 2. $Fm^{255}$ $\alpha$-singles spectrum measured with a 6-mm-diam semiconductor detector at a source-to-detector geometry of 0.2% of $4\pi$. The $\alpha$ peaks are denoted by the excited-state energy measured from $\alpha$ spectroscopy alone, and these may differ slightly from the best values obtained from $\gamma$-ray and $e^-$ spectroscopy.

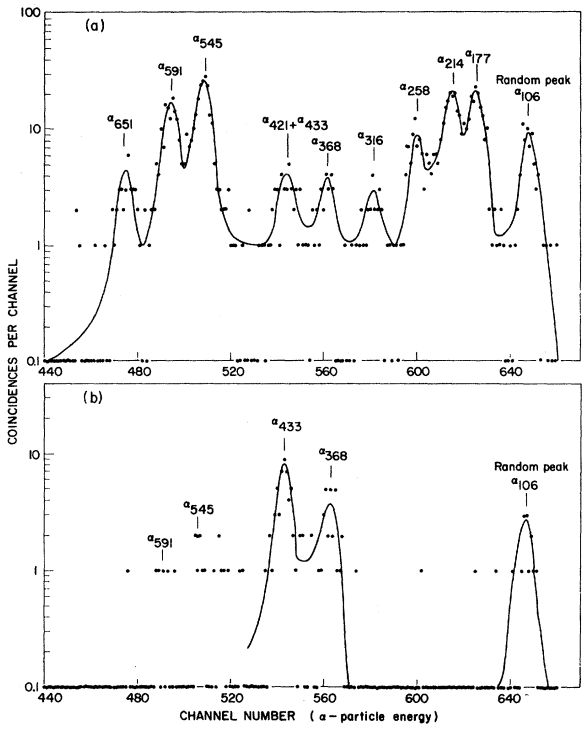


FIG. 3. $Fm^{255}$ $\alpha$ spectrum measured in coincidence ($2\tau=2$ $\mu$sec) with $\gamma$ rays. The $\alpha$ particles were detected with a 6-mm-diam semiconductor detector and the photons were detected with a 25-$cm^3$Ge(Li) diode. (a) represents an $\alpha$ spectrum gated by the Cf $K_\alpha$ x rays and (b) represents an $\alpha$ spectrum gated by the 204.1-keV photopeak. The few coincidence events below $\alpha_{433}$ are due to the presence in the 204.1-keV gate of Compton scattered photons from higher-energy $\gamma$ rays. Zero events are plotted at 0.1

$\alpha_{368}$ (6.765 MeV) and $\alpha_{433}$ (6.701 MeV) are the only observable $\alpha$ groups in coincidence with the 204.1-keV $\gamma$ ray. These $\alpha$ groups have also been observed by Milsted, Hansen, and Jaffey[10] in a spectrum measured with a magnetic spectrograph. They report the energies and abundances of these groups as 6.764 MeV (~0.019%) and 6.704 MeV (~0.031%). The intensities of the $\alpha$ groups observed in coincidence with $\gamma$ rays were obtained by making corrections for the efficiency of $\gamma$-ray detection and taking all $\gamma$ rays and x rays originating from that level into account. The $\alpha$-particle energies, intensities, and hindrance factors obtained from the present investigations are given in Table I. The $\alpha$-decay hindrance factors were calculated from the spin-independent theory of Preston.[11]

### B. $\gamma$-Ray Spectroscopy

Several $\gamma$-singles spectra of $Fm^{255}$ were measured with a 4- and a 25-$cm^3$ Ge(Li) detector. Figures 4 and 5 represent the $\gamma$-singles spectra taken with the 4-$cm^3$ Ge(Li) diode. For the spectrum shown in Fig. 4, the source contained ~$5\times10^6$ $\alpha$ dis/min of $Fm^{255}$ and was placed ~2 cm away from the detector. For the spectrum shown in Fig. 5, the source contained ~$5\times10^7$ $\alpha$ dis/min of $Fm^{255}$ and was placed next to a 1-g/$cm^2$ Al absorber abutting the detector. The peaks in Fig. 5 labeled "Cf $K$-x-ray–$K$-x-ray sum peaks" have correct intensities for sum peaks and do not contain appreciable amounts of any $\gamma$ ray. The individual components of the peak at 131.0 keV (two $\gamma$ rays and $K\beta_1'$ and $K\beta_2'$ x rays) were identified in an $\alpha$-$\gamma$ coincidence experiment (see Sec. III D). The peak at 332.0 keV

TABLE I. $Fm^{255}$ $\alpha$ groups.

| $\alpha$-particle energy (MeV) | Excited-state energy (keV) | Intensity (%) | Hindrance factor |
|---|---|---|---|
| 7.127±0.004 | 0 | 0.08±0.01 | $3.8\times10^3$ |
| 7.102±0.004 | 25 | 0.11±0.01 | $2.2\times10^3$ |
| 7.080±0.004 | 48 | 0.47±0.04 | $4.2\times10^2$ |
| 7.023±0.003 | 106 | 93.3±0.3 | 1.2 |
| 6.965±0.003 | 165 | 5.2±0.1 | 12.5 |
| 6.953±0.004 | 177 | $(2.0\pm0.4)\times10^{-2}$ | $2.9\times10^3$ |
| 6.917±0.004 | 214 | $(2.0\pm0.4)\times10^{-2}$ | $2.0\times10^3$ |
| 6.893±0.003 | 238 | 0.61±0.04 | 53 |
| 6.873±0.004 | 258 | $(1.0\pm0.2)\times10^{-2}$ | $2.6\times10^3$ |
| 6.816±0.004 | 316 | $\sim2\times10^{-3}$ | $7.4\times10^3$ |
| 6.807±0.003 | 325 | 0.11±0.01 | $1.2\times10^2$ |
| 6.765±0.004 | 368 | $(1.8\pm0.4)\times10^{-2}$ | $4.9\times10^2$ |
| 6.713±0.004 | 421 | $\sim2\times10^{-2}$ | $2.6\times10^2$ |
| 6.701±0.004 | 433 | $(3.6\pm0.7)\times10^{-2}$ | $1.3\times10^2$ |
| 6.591±0.004 | 545 | $(1.8\pm0.3)\times10^{-2}$ | 78 |
| 6.546±0.004 | 591 | $(1.3\pm0.3)\times10^{-2}$ | 66 |
| 6.487±0.004 | 651 | $(3.0\pm0.7)\times10^{-3}$ | $1.5\times10^2$ |

is also complex and consists of 332.0-, 330.0-, and 328.0-keV $\gamma$ rays. The 330.0- and 332.0-keV $\gamma$ rays have also been observed in an $\alpha$-$\gamma$ coincidence experiment. The small peaks with question marks indicate that we are not certain that they are $Fm^{255}$ $\gamma$ rays.

The best values of the $\gamma$-ray energies and intensities obtained from several spectra are given in Table II. The intensities of the intense $\gamma$ rays, in terms of photons per $Fm^{255}$ $\alpha$ decay, were obtained by counting the $\gamma$-ray spectrum of a thin sample and determining its $\alpha$ dis/min with a low-geometry counter. The positions of the transitions in the decay scheme (Fig. 6), as given in column 3 of Table II, are based on the results of the multiparameter coincidence experiments. The intensity of the 152.8-keV peak relative to that of the 177.7-keV peak associated with the $\alpha$ decay of $Fm^{255}$ is ~10% greater than the intensity measured[4] in the electron-capture decay of $Es^{251}$. As the same Ge(Li) detector was used for measuring the $\gamma$-ray spectrum of both nuclides, the additional intensity in the 152.8-keV peak is due to the 258.4 → 105.73 transition (152.7 keV).

### C. Electron Spectroscopy

#### *1. Instrumental*

The conversion-electron spectrum was surveyed from 3 to 130 keV and at certain selected higher-energy regions on the Argonne iron-free toroidal spectrometers operated in tandem. In this mode of operation the source is imaged by the first spectrometer in the plane midway between the two coils; this image is the effective source for the second machine. This provides twice the dispersion of a single spectrometer. A source diameter of 6 mm and final detector aperture of 7.2 mm diam yield an instrumental resolution of 0.3% full width at half maximum in momentum and a transmission of 8.5% of $4\pi$.

The source was made by subliming Fm as the chloride in vacuum from a Ta filament onto an Al backing with a 6-mm-diam mask defining the deposit. Systematic broadening of lines with decreasing energy below 80 keV attested to the presence of extraneous material (most probably Ta) on the faintly visible source. Figure 7 shows a count-vs-momentum spectrum. This figure should not be used to make intensity comparisons since large source-decay and electron-detection efficiency corrections have not been applied to this spectrum.

#### *2. Line Energies*

Because of the source-thickness effects, line positions were determined from the intercept of the high-energy edge with the local continuum of scattered electrons. However, the advantage of peak-position determination in a complex spectrum was retained by plotting the ratio of peak position to high-edge position as a function of electron energy for 22 of the cleaner lines over the whole energy range. This allows the peak position to be corrected for the source-thickness distortion at any energy. Peak shift relative to high-energy-

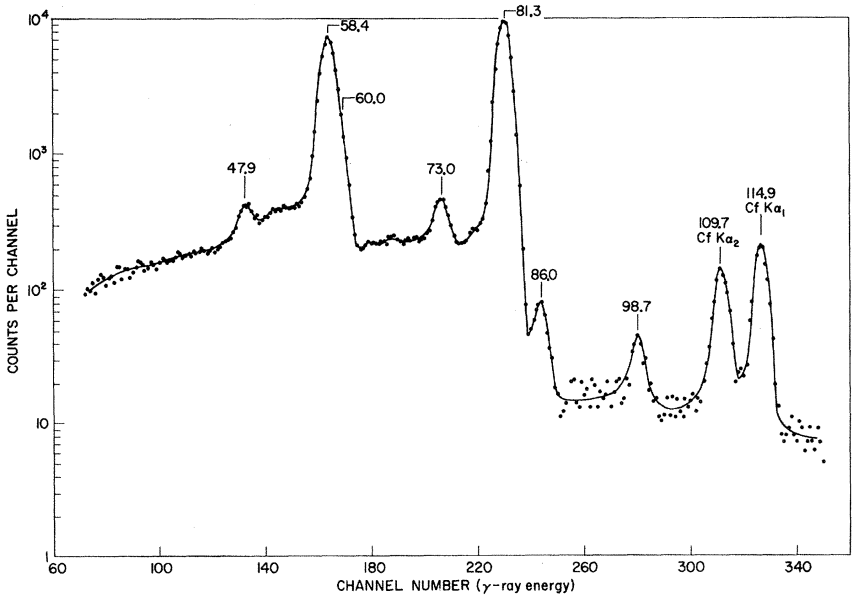


FIG. 4. Low-energy portion of the $Fm^{255}$ $\gamma$-ray spectrum measured with a 4-$cm^3$ coaxial Ge(Li) detector. The source containing ~$5\times10^6$ $\alpha$ dis/min of $Fm^{255}$ was placed 2 cm away from the detector.

edge intercept, due to source thickness, was negligible at 100 keV, amounted to $\sim 1\times10^{-3}$ (momentum) at 40 keV, and $\sim 1\times10^{-2}$ (momentum) at 5 keV. Uncertainties in line positions were assigned taking into account statistical quality, unfolding, and source-effect corrections. Spectrometer calibration error (5 parts in $10^5$) was small compared to other uncertainties.

### *3. Binding Energies*

Tabulated atomic-electron binding energies[12,13] in the daughter californium available did not yield consistent energies for a given transition when added to the various conversion lines from that transition. In order to arrive at better values for these binding energies, both the binding and transition energies were treated as parameters in a weighted least-squares computer-adjustment procedure. Thirty-seven of the better lines from nine transitions[14] generated equations of the form

$$E_i + BE_j - \gamma_k = \delta_i ,$$

where $E_i$ is the conversion-line energy, $BE_j$ is the appropriate binding energy to yield transition energy $\gamma_k$, and $\delta_i$ is a residual. Three additional equations of the form $\gamma_j+\gamma_k-\gamma_m=\delta_i$ were included; these express the crossover-sum relationships in the decay scheme (24.8 + 23.0 − 47.8; 23.0 + 58.5 − 81.5; 60 + 73 − 133).

The function

$$s=\sum_i w_i(\delta_i)^2$$

was then minimized[15] with respect to the 19 variable parameters (9 $\gamma$-ray energies and 10 binding energies). Weights $w_i=\sigma_i^{-2}$ were obtained from the assigned uncertainties in the conversion-line energies ($E_i\pm\sigma_i$) in the case of the 37 line-generated equations, whereas the weights assigned to the three crossover-sum equations were derived from uncertainties in the transition energies assigned on the basis of the $\sigma_i$ of the various con-

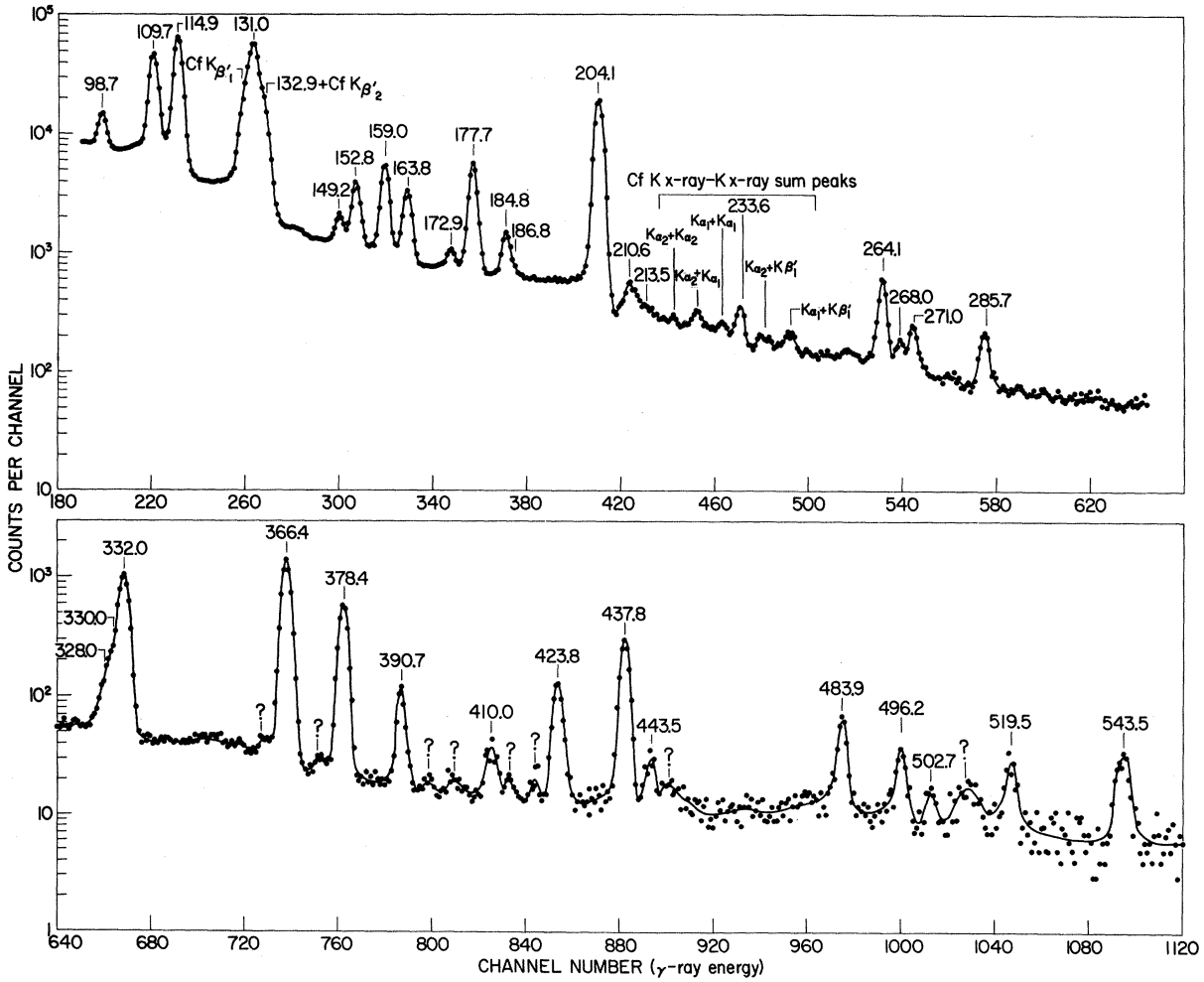


FIG. 5. High-energy portion of the $Fm^{255}$ $\gamma$-ray spectrum measured with a 4-$cm^3$ coaxial Ge(Li) detector. The source ($\sim 5\times10^7$ $\alpha$ dis/min) was placed next to a 1-g/$cm^2$ Al absorber abutting the detector.

TABLE II. $Fm^{255}$ $\gamma$ rays.

| Energy (keV) | Intensity [photons/($10^2$ $Fm^{255}$ $\alpha$ decays)] | | Transition |
|---|---|---|---|
| 47.9±0.1 | (1.9 ±0.2)×$10^{-2}$ | | 47.83→ 0 |
| 58.4±0.1 | 0.78±0.06 | | 105.73→ 47.83<br>+106.30→ 47.83 |
| 60.0±0.1 | 0.12±0.016 | | 166.31→106.30 |
| 63.8±0.5 | (8 ±3)×$10^{-4}$ | | 434.2→ 370.4 |
| 73.0±0.1 | (2.9 ±0.2)×$10^{-2}$ | | 239.33→ 166.31 |
| 81.3±0.1 | 1.08±0.07 | | 105.73→ 24.82<br>+106.30→ 24.82 |
| 86.0±0.1 | (6.6 ±0.6)×$10^{-3}$ | | 325.3→ 239.33 |
| 98.7±0.2 | (2.9 ±0.2)×$10^{-3}$ | $1.9\times10^{-3}$<br>$1.0\times10^{-3}$ | 146.5→ 47.83<br>+424.1→ 325.3 |
| 109.7±0.1 | (1.95±0.14)×$10^{-2}$ | | Cf $K_{\alpha_2}$ |
| 114.9±0.1 | (2.8 ±0.2)×$10^{-2}$ | | Cf $K_{\alpha_1}$ |
| 129.3±0.2 | (1.1 ±0.15)×$10^{-2}$ | | Cf $K_{\beta_1'}$ |
| 131.0±0.2 | (2.8 ±0.3)×$10^{-2}$ | | 370.4→ 239.33 |
| 132.9±0.2 | (8.5 ±0.9)×$10^{-3}$ | | 239.33→ 106.30 |
| 133.4±0.2 | (4.1 ±0.7)×$10^{-3}$ | | Cf $K_{\beta_2'}$ |
| 149.2±0.2 | (6.5 ±0.6)×$10^{-4}$ | | 295.7→ 146.5 |
| 152.8±0.2 | (2.1 ±0.2)×$10^{-3}$ | $1.9\times10^{-3}$<br>$0.2\times10^{-3}$ | 177.7→ 24.82<br>+258.4→105.73 |
| 159.0±0.2 | (3.6 ±0.4)×$10^{-3}$ | | 325.3→ 166.31 |
| 163.8±0.2 | (2.0 ±0.2)×$10^{-3}$ | | 211.6→ 47.83 |
| 172.9±0.2 | (3.0 ±0.3)×$10^{-4}$ | | 319.4→ 146.5 |
| 177.7±0.2 | (4.8 ±0.4)×$10^{-3}$ | | 177.7→ 0 |
| 184.8±0.2 | (8.0 ±0.8)×$10^{-4}$ | | 424.1→ 239.33 |
| 186.8±0.3 | (1.0 ±0.2)×$10^{-4}$ | | 211.6→ 24.82 |
| 204.1±0.2 | (2.4 ±0.2)×$10^{-2}$ | | 370.4→166.31 |
| 210.6±0.3 | (3.0 ±0.4)×$10^{-4}$ | | 258.4→ 47.83 |
| 213.5±0.4 | ~1×$10^{-4}$ | | 319.4→ 105.73 |
| 233.6±0.3 | (2.6 ±0.5)×$10^{-4}$ | | 258.4→ 24.82 |
| 264.1±0.2 | (1.0 ±0.1)×$10^{-3}$ | | 370.4→ 106.30 |
| 268.0±0.5 | (1.8 ±0.4)×$10^{-4}$ | | 434.2→ 166.31 |
| 271.0±0.3 | (3.2 ±0.4)×$10^{-4}$ | | 590.2→ 319.4 |
| 285.7±0.3 | (3.9 ±0.4)×$10^{-4}$ | | 544.1→ 258.4 |
| 328.0±0.5 | (2.3 ±0.4)×$10^{-4}$ | | 434.2→ 106.30 |
| 330.0±0.5 | (4.4 ±0.8)×$10^{-4}$ | | 649.1→ 319.4 |
| 332.0±0.4 | (3.3 ±0.4)×$10^{-3}$ | | 544.1→ 211.6<br>+590.2→ 258.4 |
| 366.4±0.2 | (5.0 ±0.5)×$10^{-3}$ | | 544.1→ 177.7 |
| 378.4±0.2 | (2.3 ±0.3)×$10^{-3}$ | | 590.2→ 211.6 |
| 390.7±0.5 | (4.0 ±0.8)×$10^{-4}$ | | 649.1→ 258.4 |
| 410.0±0.5 | (1.2 ±0.4)×$10^{-4}$ | | 649.1→ 239.33 |
| 423.8±0.2 | (6.0 ±0.6)×$10^{-4}$ | | 590.2→ 166.31 |
| 437.8±0.2 | (1.35±0.14)×$10^{-3}$ | | 544.1→ 106.30 |
| 443.5±0.5 | ~5×$10^{-5}$ | | 590.2→ 146.5 |
| 483.9±0.3 | (3.9 ±0.4)×$10^{-4}$ | | 590.2→ 106.30 |
| 496.2±0.4 | (1.7 ±0.4)×$10^{-4}$ | | 544.1→ 47.83 |
| 502.7±0.5 | ~4×$10^{-5}$ | | 649.1→ 146.5 |
| 519.5±0.5 | (1.5 ±0.4)×$10^{-4}$ | | 544.1→ 24.82 |
| 543.5±0.5 | (2.4 ±0.6)×$10^{-4}$ | | 544.1→ 0<br>+590.2→ 47.83 |

version lines of the particular transition in question.

The binding energies thus derived (Table III, column 2) are significantly different from the Bearden and Burr[12] tabulated values for the $K$ (from $L_2$, $L_3$, and $K\alpha$ x rays), $L_1$, $L_2$, $L_3$, and $M_2$ shells. In Table III, column 4 we present our own graphical extrapolations[16] (from $Z = 92$, 93, 95, and from experimental data of Hollander *et al.*[17] at $Z = 97$) for $Z = 98$ which are generally higher than our de-

rived values but significantly different only for the $L_3$ shell.

### 4. *Intensities*

Relative conversion-line areas were obtained from width and height measurements with an energy-dependent correction for source-thickness tailing obtained from a few of the lines where the low-energy tail was clear.

Other corrections were made for the efficiency of the bare cleaved-crystal-surface NaI(Tl) scintillation detector,[18] for decay of $Fm^{255}$ (measurements covered up to 3.5 half-lives) and for spectrometer transmission. We assigned an over-all uncertainty of ~20% to the intensity per $\alpha$ decay unless statistical uncertainty of a particular line exceeded this estimate.

A test of the absolute intensity measurements is available from a comparison of the sum of the 24.8- and 47.8-keV transitions with the absolute $\alpha$ count on the sample, since there is only ~0.1% $\alpha$ feed to the ground state. The electron line intensities predicted $(5 \pm 1) \times 10^6$ dis/min; the absolute $\alpha$ count gave $(3.4 \pm 0.1) \times 10^6$ dis/min. This indicates a systematic error which is not understood. In another test the experimental internal-conversion coefficients (calculated using the absolute $e^-$ intensities and the absolute $\gamma$ intensities) were compared with theoretical values[19] for eight lines in the 60-(96% $M1$), 73-(96% $M1$), 80.9-($E2$), and 81.5-keV ($E2$) transitions. This showed the experimental values average about 20% larger than theoretical values. The discrepancy here is not as large as in the first test where lower-energy lines contribute more heavily. It is probable that one of the energy-dependent correction factors (tail or efficiency) is overcompensating the lower-energy lines.

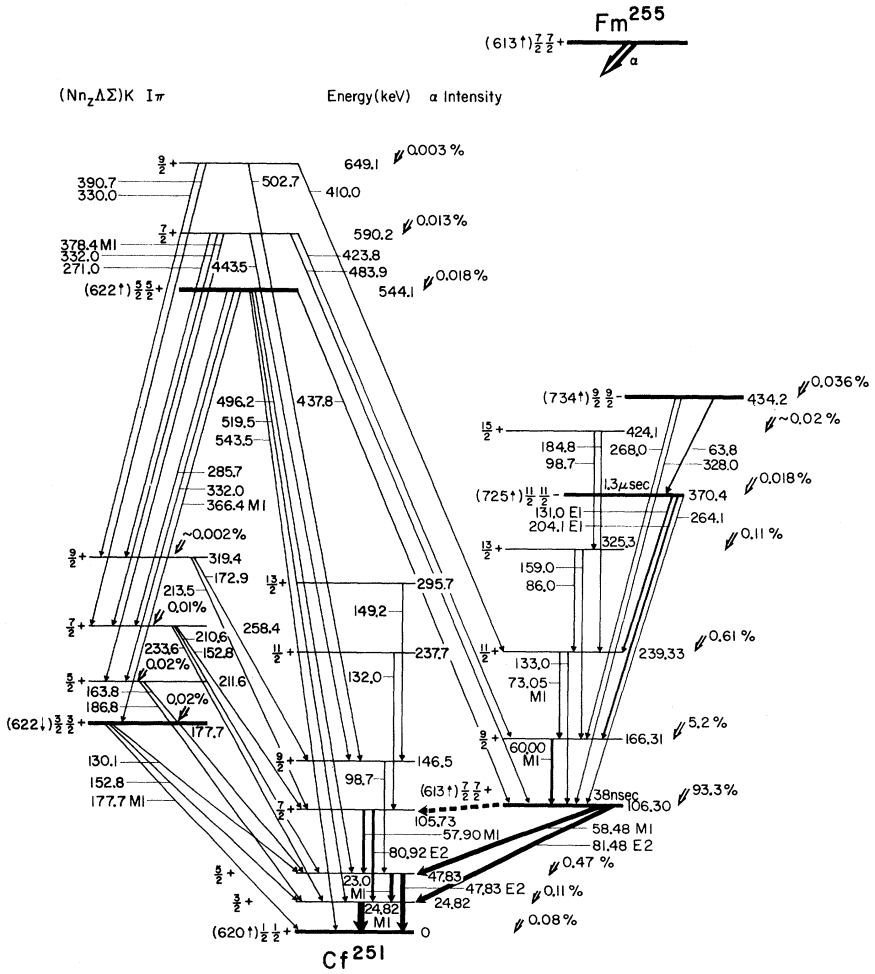


FIG. 6. $Fm^{255}$ $\alpha$-decay scheme constructed on the basis of the present investigation. Each rotational band built on a Nilsson state is shown in a different vertical column, with the band head emphasized and labeled with the asymptotic quantum numbers.

In view of this discrepancy we quote in Table IV the intensity of $e^-$ lines compared with the sum of the $e^-$ intensities of the 24.8- and 47.8-keV transitions as 100%. At each level the total out feed $(\gamma+e^-)$ minus total in feed $(\gamma+e^-)$ must equal the $\alpha$ feed to that level. For example, at the 106.30- and 105.73-keV levels the $(e^-+\gamma)$ intensity balance predicts $(98\pm 20)\%$, whereas the $\alpha$ spectroscopy gives 93% of the $\alpha$ decay to these levels. Similarly at all other levels the relatively crude $e^-$ intensity data yield no disagreement with the $\alpha$ spectroscopy intensities. The multipolarities of the transitions, as given in the last column of Table IV, are deduced from subshell ratios. In general, the subshell ratios are subject to less uncertainty than the absolute conversion coefficients. Only an upper limit for the intensities of the 131.0- and 204.1-keV $K$ and $L$ lines was obtained which is consistent only with their being $E1$ transitions.

Attempts were also made to unfold the complicated $L$ auger spectrum in the region between 8 and 16 keV. About 25 lines are evident with varying degrees of certainty. In Fig. 7 we have indicated some assignments which are more certain.

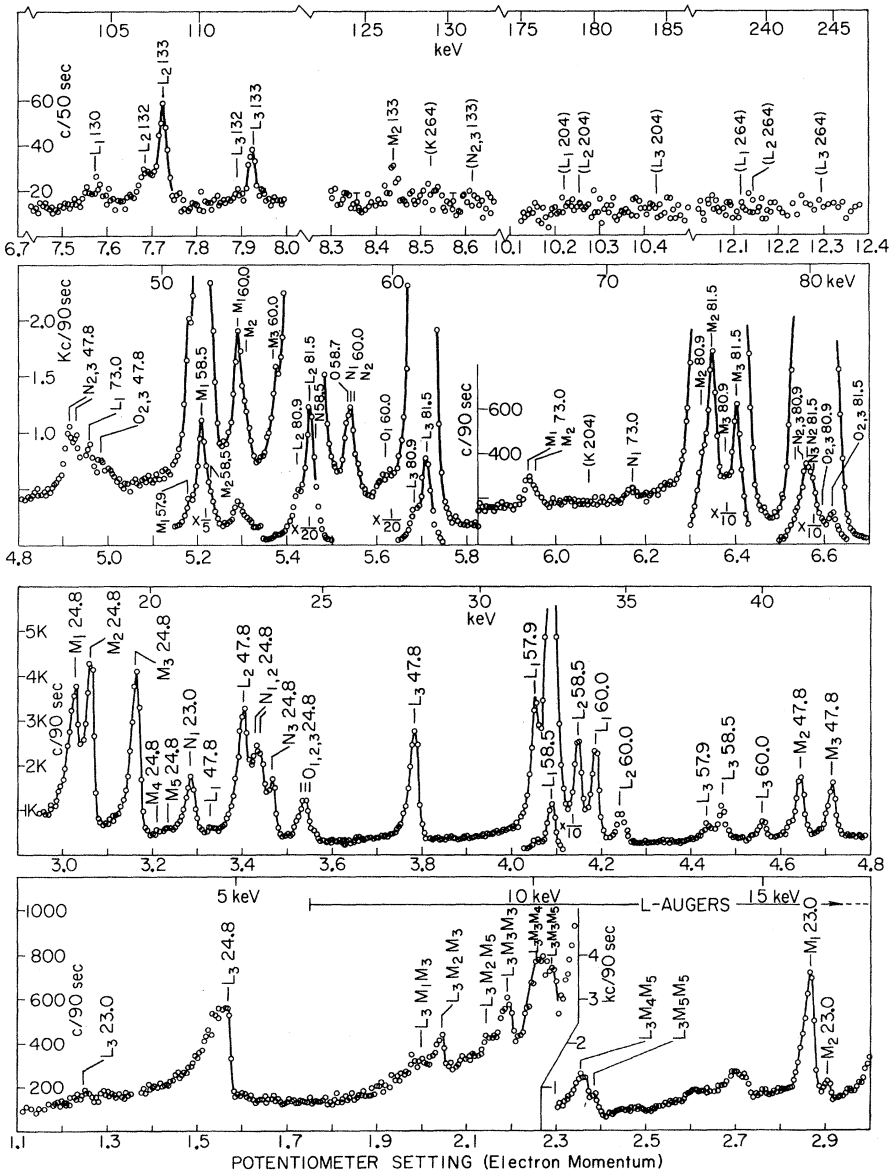


FIG. 7. A count-vs-momentum plot showing the electron lines associated with the $\alpha$ decay of $Fm^{255}$. No decay or efficiency corrections have been applied to the plot and as such it should not be used as a measure of relative intensities. Parentheses indicate where only an upper limit of intensity has been obtained. The region between 6.7 and 7.4 potentiometer units was featureless and is not shown here.

TABLE III. Atomic-electron binding energies in californium ($Z=98$).

| Shell | Binding energy (keV) Present work | Bearden and Burr [a] | Our graphical extrapolation [b] |
|---|---|---|---|
| $K$ | 134.8 ±0.1 [c] | 135.960 | 134.92 ±0.060 |
| $L_1$ | 25.996±0.013 | 26.110 | 26.005±0.025 |
| $L_2$ | 25.098±0.013 | 25.250 | 25.115±0.025 |
| $L_3$ | 19.881±0.013 | 19.930 | 19.935±0.030 |
| $M_1$ | 6.737±0.010 | 6.754 | 6.778±0.030 |
| $M_2$ | 6.316±0.012 | 6.359 | 6.345±0.045 |
| $M_3$ | 5.089±0.015 | 5.109 | 5.115±0.045 |
| $N_1$ | 1.799±0.015 | 1.799 | 1.817±0.035 |
| $N_2$ | 1.609±0.020 | 1.616 | |
| $N_3$ | 1.288±0.015 | 1.279 | |
| $O_1$ | | 0.419 | 0.409±0.035 |
| $O_{2,3}$ | 0.299±0.020 | | |

[a] J. A. Bearden and A. F. Burr (Ref. 12) citing self-consistent field calculations of D. Liberman *et al.*, Phys. Rev. 137, 27 (1965).

[b] Not including present derived values but relying on the experimental data of Hollander *et al.* (see Ref. 17) at $Z=97$.

[c] From $K$ x-ray energies measured with a Ge(Li) detector (Table II) and $L_{2,3}$ binding energies shown in this table.

*5. Multipolarities of High-Energy Transitions*

To measure the multipolarities of higher-energy transitions, an $\alpha$-$e^-$ coincidence experiment was carried out. A cooled Si(Li) detector coupled with a low-noise preamplifier was used to detect the electrons; the $\alpha$ particles, after passing through the source backing (200-$\mu$g/cm$^2$ Al), were detected with a 2-cm$^2$ semiconductor detector. The $\alpha$ detector and $e^-$ detector were placed at an angle of 180° with respect to each other and had geometries of 10 and 2%, respectively. The resolving time ($2\tau$) of the coincidence circuit was 300 nsec. In an $e^-$ spectrum measured in coincidence with all $\alpha$ particles below 6.90 MeV, only $K$ lines of the 332-, 366-, and 378-keV transitions were identified. The $K$ conversion coefficients of these transitions were found to be 1.1±0.3, 0.9±0.3, and 0.8±0.3, respectively. These values are in good agreement with the theoretical values[19] for $M1$ transitions (1.1, 0.83, and 0.76, respectively). Other electron lines were too weak to be observed.

**D. Two-Parameter Coincidence Measurements**

*1. $\alpha$-$\gamma$ Coincidences*

An $\alpha$-$\gamma$ coincidence experiment using a two-parameter analyzer was performed in order to correlate the $\gamma$ transitions with specific $\alpha$ groups. A 6-mm-diam semiconductor detector was used to detect the $\alpha$ particles and the $\gamma$ rays were detected with a 25-cm$^3$ Ge(Li) detector. The resolving time of the coincidence circuit was 2 $\mu$sec. The coincidence events were accumulated on a magnetic tape and were later read back into the memory through a digital gate system. Thus either $\alpha$ or $\gamma$ spectra could be obtained in coincidence with selected gates. The $\alpha$ spectra in coincidence with the Cf $K_\alpha$ ($K_{\alpha 2}+K_{\alpha 1}$) and the 204.1-keV $\gamma$ ray have already been shown in Sec. III A. The $\gamma$-ray spectra in coincidence with the $\alpha_{238}$, $\alpha_{368}$, and $\alpha_{433}$ are shown in Fig. 8. The $\alpha$ gate for each peak included ~25 keV on either side of the peak. The results of this experiment are given in Table V. The correlation of each $\gamma$ ray with a specific $\alpha$ group was ascertained by varying the gate to include higher- or lower-energy $\alpha$ particles. The fact that each $\alpha$ peak contained some tailing due to higher-energy $\alpha$ peaks was also taken into account.

By comparing the $\gamma$-singles spectrum with that taken in coincidence ($2\tau=2$ $\mu$sec) with all $\alpha$ particles, it was learned that only ~50% of the 131.0- and 204.1-keV $\gamma$ rays were in coincidence with $\alpha$ particles. This indicates that the half-life of their parent state is long and is comparable to the resolving time of the circuit ($2\tau=2$ $\mu$sec). Figure 8 (b) shows that the 131.0- and 204.1-keV $\gamma$ rays originate from the 370.4-keV level. The fact that these $\gamma$ rays are also the main $\gamma$ rays in coincidence with the $\alpha_{433}$ suggests that the 434.2-keV level deexcites through the 370.4-keV level. The presence of a 63.8-keV $\gamma$ ray [Fig. 8(c)] further confirms this hypothesis. From the $\alpha$ population to the 434.2-keV level (0.036%) and the intensity of the 63.8-keV $\gamma$ ray (~0.0008%) one obtains a total conversion coefficient of 44±17. The theoretical values[19] for a 63.8-keV transition are: $M1$, 36; $E2$, 190; and $E1$, 0.5. This suggests that the 63.8-keV transition is predominantly $M1$.

A large amount of Cf $K$ x rays were observed in coincidence with $\alpha$ particles populating the rotational bands built at 177.7- and 544.1-keV levels. Only the 177.7- and 152.8-keV $\gamma$ rays and Cf $K$ x rays were observed in coincidence with the $\alpha_{178}$ group. The ratio of the $K$ x-ray intensity to the combined intensity of the 152.8- and 177.7-keV $\gamma$ rays was found to be 6±2. This agrees with the theoretical value[19] of 7.0 for $M1$ transitions. Thus, the multipolarities of the 177.7- and 152.8-keV transitions are mainly $M1$ (with perhaps some $E2$ admixture).

*2. $\gamma$-$\gamma$ Coincidences*

A $\gamma$-$\gamma$ coincidence experiment using a two-par-

TABLE IV. Conversion electrons and $\gamma$ rays associated with $\alpha$ decay of $Fm^{255}$.

| Transition energy (initial→final levels) (keV) | Shell | $e^-$ energy [keV ± (eV)] | Transition energy [keV ± (eV)] | Intensity [a] %/decay | Multipolarity and subshell data from which derived |
|---|---|---|---|---|---|
| 23.001 ± 0.017 | $M_1$ | 16.265 (15) | 23.002 (20) | 17 | $M1 > 99.8\%$ |
| (47.83 → 24.82) | $M_2$ | 16.690 (20) | 23.006 (25) | 2.2 | $M_1/M_2$ |
| | $N_1$ | 21.216 (20) | 22.995 (25) | 5 | |
| | | | | 24 | |
| | $L_3$ | 4.936 (35) | 24.817 (35) | 24 | |
| | $M_1$ | 18.099 (27) | 24.836 (30) | 11 | |
| | $M_2$ | 18.503 (17) | 24.819 (20) | 16 | $M1(93 \pm 2)\%$ |
| 24.824 ± 0.015 | $M_3$ | 19.731 (17) | 24.820 (20) | 14 | |
| (24.82 → 0) | $M_4$ | 20.37 (60) | 24.86 (60) | 0.4 ± 0.2 | $M_1/M_2$ |
| | $M_5$ | 20.59 (60) | 24.84 (60) | 0.4 ± 0.4 | $M_2/M_3$ |
| | $N_1$ | 23.075 (30) | 24.854 (35) | 8 | |
| | $N_2$ | 23.213 (30) | 24.822 (35) | | |
| | $N_3$ | 23.529 (17) | 24.817 (25) | 3.7 | |
| | $O_{1,2,3}$ | 24.509 (30) | 24.839 (35) | 3.5 | |
| | | | | 81 | |
| | $L_1$ | 21.81 (70) | 47.81 (70) | 0.51 | |
| | $L_2$ | 22.735 (16) | 47.833 (20) | 8.0 | |
| 47.830 ± 0.015 | $L_3$ | 27.942 (10) | 47.823 (20) | 5.1 | $E2 > 80\%$ |
| (47.83 → 0) | $M_1$ | 41.11 (90) | 47.84 (90) | 0.10 ± 0.05 | $L_1/L_3$ |
| | $M_2$ | 41.527 (18) | 47.843 (25) | 1.6 | $M_1/M_3$ |
| | $M_3$ | 42.744 (9) | 47.833 (20) | 1.4 | |
| | $N_2$ | 46.221 (18) | 47.830 (35) | 0.29 | |
| | $N_3$ | 46.555 (18) | 47.843 (35) | 0.34 | |
| | $O_{2\,3}$ | 47.529 (19) | 47.828 (35) | 0.31 | |
| | $\gamma$ | | 47.8 | 0.019 | |
| | | | | 17.6 | |
| | $L_1$ | 31.911 (16) | 57.907 (25) | 4.0 | $M1 > 95\%$ |
| 57.902 ± 0.015 | $L_3$ | 38.015 (17) | 57.896 (20) | 0.5 | $L_1/L_3$ |
| (105.73 → 47.83) | $M_1$ | 51.14 (100) | 57.87 (100) | 0.6 ± 0.2 | |
| | $\gamma$ | | | 0.11 | |
| | | | | 5.2 | |
| | $L_1$ | 32.486 (16) | 58.482 (20) | 23 | |
| | $L_2$ | 33.377 (9) | 58.475 (15) | 3.5 | $M1 > 98.5\%$ |
| 58.477 ± 0.015 | $L_3$ | 38.609 (17) | 58.490 (20) | 1.0 | $L_1/L_3$ |
| (106.30 → 47.83) | $M_1$ | 51.738 (10) | 58.475 (15) | 6.0 | |
| | $M_2$ | 52.12 (100) | 58.44 (100) | | |
| | $\gamma$ | | 58.4 | 0.67 | |
| | | | | 34.2 | |
| | $L_1$ | 34.003 (9) | 59.999 (15) | 3.4 | $M1 > 94\%$ |
| | $L_2$ | 34.895 (16) | 59.993 (20) | 1.0 | |
| 60.004 ± 0.015 | $L_3$ | 40.131 (10) | 60.012 (15) | 0.5 | $L_1/L_2$ |
| (166.31 → 106.30) | $M_1$ | 53.280 (20) | 60.030 (25) | 1.5 | $L_1/L_3$ |
| | $M_2$ | 53.65 (100) | 59.98 (100) | | |
| | $M_3$ | 54.84 (100) | 59.95 (100) | (0.2 ± 0.1) | |
| | $N_1$ | 58.24 (60) | 60.04 (60) | (0.4 ± 0.2) | |
| | $\gamma$ | | | 0.12 | |
| | | | | 7.1 | |
| 73.046 ± 0.025 | $L_1$ | 47.064 (20) | 73.060 (25) | 0.30 | |
| (239.33 → 166.31) | $M_1$ | 66.279 (45) | 73.016 (45) | 0.11 | $M1 > 96\%$ |
| | $M_2$ | | | <0.025 | |
| | $N_1$ | 71.34 (220) | 73.12 (220) | 0.022 | $M_1/M_2$ |
| | $\gamma$ | | | 0.029 | |
| | | | | 0.46 | |

TABLE IV *(Continued)*

| Transition energy (initial → final levels) (keV) | Shell | $e^-$ energy [keV ± (eV)] | Transition energy [keV ± (eV)] | Intensity [a] %/decay | Multipolarity and subshell data from which derived |
|---|---|---|---|---|---|
| | $L_1$ | | | (0.2 ± 0.1) | |
| 80.920 ± 0.045 | $L_2$ | 55.836 (60) | 80.934 (60) | 4.5 | $E2$ |
| (105.73 → 24.82) | $L_3$ | 61.060 (60) | 80.941 (60) | 3.6 | ($M1 < 20\%$) |
| | $M_2$ | 74.66 (110) | 80.98 (110) | (1.9) | $L_2/L_3$ |
| | $M_3$ | 75.83 (230) | 80.92 (230) | 1.1 | |
| | $N_2$ | | | (0.9) | |
| | $N_3$ | | | | |
| | $O_{2,3}$ | | | (0.2) | |
| | $\gamma$ | | | 0.27 | |
| | | | | 12.5 | |
| | $L_1$ | | | (1.1) | $E2$ |
| | $L_2$ | 56.395 (20) | 81.493 (25) | 20 | ($M1 < 20\%$) |
| 81.477 ± 0.020 | $L_3$ | 61.599 (20) | 81.480 (25) | 13 | $L_2/L_3$ |
| (106.30 → 24.82) | $M_1$ | | | (0.3) | |
| | $M_2$ | 75.136 (25) | 81.452 (30) | 5.8 | |
| | $M_3$ | 76.376 (25) | 81.465 (30) | 3.9 | |
| | $N_2$ | 79.87 (70) | 81.48 (70) | (3.6) | |
| | $N_3$ | 80.28 (120) | 81.56 (120) | | |
| | $O_{2,3}$ | 81.19 (70) | 81.49 (70) | 0.8 | |
| | $\gamma$ | | | 0.81 | |
| | | | | 49.3 | |
| 130.10 ± 0.26 | $L_1$ | 104.10 (260) | 130.10 (260) | 0.0036 ± 0.0012 | |
| (177.7 → 47.83) | $L_{2,3}$ | | | <0.0012 | |
| 131.0 ± 0.2 | $L_{1,2,3}$ | | | <0.0014 | $E1$ |
| (370.4 → 239.33) | $\gamma$ | | 131.1 (200) | 0.028 | $L_1$ and $L_2$ conversion coefficients <0.05 |
| 132.03 ± 0.13 | $L_2$ | 106.90 (130) | 132.00 (130) | 0.0047 | |
| (237.7 → 105.73) | $L_3$ | 112.17 (130) | 132.05 (130) | 0.0026 ± 0.0009 | |
| | $\gamma$ | | | 0.0021 | |
| 133.01 ± 0.050 | $L_2$ | 107.93 (50) | 133.02 (50) | 0.0176 | |
| (239.33 → 106.30) | $L_3$ | 113.05 (50) | 132.93 (50) | 0.0091 | |
| | $M_2$ | 126.70 (140) | 133.01 (140) | 0.0067 ± 0.0020 | |
| | $\gamma$ | | | 0.0064 | |
| 204.1 | $K$ | | | <0.01 | $E1$ |
| (370.4 → 166.31) | $L_{1,2,\text{or } 3}$ | | | <0.004 | $L_1$ and $L_2$ conversion coefficients <0.17 |
| | $\gamma$ | | 204.1 (200) | <0.024 | |
| 264.1 | $K$ | | | <0.006 | |
| (370.4 → 106.30) | $L_{1,2,\text{or } 3}$ | | | <0.006 | |
| | $\gamma$ | | 264.1 (200) | 0.001 | |

[a] Conversion-electron intensities are uncertain to ±20% unless specifically indicated. $\gamma$-intensity errors not given here (see Table II). Values in parentheses indicate lines masked by strong lines. In these cases intensity partition is based on theoretical expectation. Intensities of unresolved $\gamma$ rays are obtained by partitioning the total $\gamma$-ray intensity in accordance with the observed electron intensity.

ameter analyzer was performed with a view to obtaining the mode of deexcitation of the high-energy $\gamma$ rays. The $\gamma$ rays were detected with 4- and 25-$cm^3$ Ge(Li) diodes. The resolving time of the coincidence unit was 2$\mu$sec. The results obtained from this experiment are given in Table VI. The $\gamma$-ray gate included only the symmetric part of the photopeak (gate width = 6 keV). The results very clearly established that the 204.1-keV transition goes to the 166.31-keV level and 131.0-keV transition deexcites to the 239.3-keV level. Also the presence of large amounts of Cf $K$ x rays in

coincidence with the 332.0- and 366.4-keV $\gamma$ rays suggests that these transitions populate the 177.7-keV rotaional band.

### E. Half-Life of the 370.4-keV State

The $\alpha$-$\gamma$ coincidence experiment (Sec. III D) established that the 131.0- and 204.1-keV $\gamma$ rays originate from the 370.4-keV level and are delayed. In another $\alpha$-$\gamma$ coincidence experiment in which the resolving time of the coincidence circuit was changed from 2 $\mu$sec to 200 nsec, less than 10% of the 131.0- and 204.1-keV $\gamma$ rays remained in coincidence with the $\alpha$ particles. As the intensity

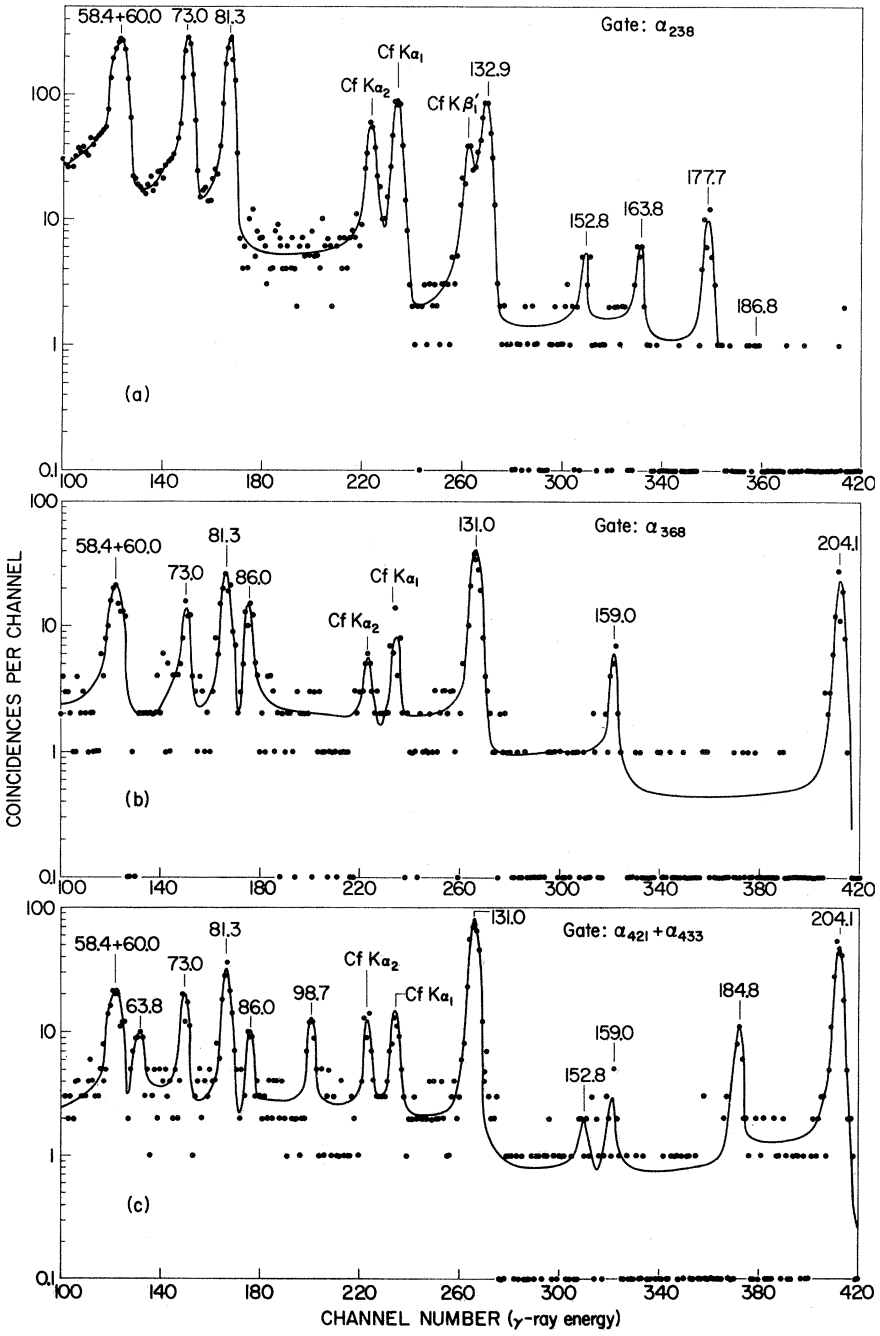


FIG. 8. $Fm^{255}$ $\gamma$-ray spectrum measured in coincidence ($2\tau = 2\mu$ sec) with: (a) $\alpha_{238}$ (6.87 to 6.92 MeV); (b) $\alpha_{368}$ (6.74 to 6.79 MeV); and (c) $\alpha_{421} + \alpha_{433}$ (6.68 to 6.73 MeV. (a) Cf $K$ x rays, 152.8-, 163.8-, and 177.7-keV $\gamma$ rays are due to the presence in the gate of $\alpha$ particles populating the 177.7-keV band. Zero events are plotted at 0.1.

TABLE V. Results of two-parameter $\gamma$-$\gamma$ coincidence experiment.

| Gate [a] | $\gamma$ rays [b] (keV) |
|---|---|
| $\alpha_{106}$ | 47.9, 58.4, and 81.3 |
| $\alpha_{146}$ | 98.7 |
| $\alpha_{166}$ | 58.4, 60.0, and 81.3 |
| $\alpha_{177}$ | Cf $K$ x rays, 152.8, and 177.7 |
| $\alpha_{214}$ | Cf $K$ x rays, 163.8, and 186.8 |
| $\alpha_{238}$ | 58.4, 60.0, 73.0, 81.3, and 132.9 |
| $\alpha_{259}$ | Cf $K$ x rays, 152.8, and 210.6 |
| $\alpha_{295}$ | 149.2 |
| $\alpha_{316}$ | Cf $K$ x rays |
| $\alpha_{325}$ | 58.4, 60.0, 73.0, 81.3, 86.0, and 159.0 |
| $\alpha_{368}$ | 58.4, 60.0, 73.0, 81.3, 131.0, 204.1, and 264.1 |
| $\alpha_{421}+\alpha_{433}$ | 58.4, 60.0, 63.8, 73.0, 81.3, 98.7, 131.0, 184.8, 204.1, and 264.1 |
| $\alpha_{545}$ | Cf $K$ s rays, 152.8, 177.7, 332.0, 366.4, and 437.8 |
| $\alpha_{591}$ | Cf $K$ x rays, 163.8, 177.7, 332.0, and 378.4 |
| $\alpha_{651}$ | Cf $K$ x rays and 390.7 |

[a] Each gate included $\alpha$ particles 25 keV on either side of the peak mentioned.
[b] The $\gamma$-ray energies in column 2 are those obtained from $\gamma$-singles spectra. The coincidences indicated by underlined $\gamma$ rays are particularly critical in the construction of the decay scheme.

of the $\alpha_{368}$ group is only half of that of the $\alpha_{433}$ group, the reduction in $\gamma$-ray intensities indicates that the 370.4-keV level is delayed.

The half-life of the 370.4-keV level was measured with a time-to-amplitude converter (TAC). The $\alpha$ particles were detected with a 2-$cm^2$ semiconductor detector and the $\gamma$ rays were detected with a 3-in.×3-in. NaI(Tl) detector. Timing single-channel analyzers were used to select $\alpha$ particles between 6.59 and 6.79 MeV and $\gamma$ rays between 160 and 230 keV. The $\alpha$ pulses and $\gamma$-ray pulses from the single-channel analyzers were used as start and stop signals for the TAC. A time spectrum collected over a period of 20 h is shown in Fig. 9. The half-life of the 370.4-keV level was determined from a least-squares-fit analysis and found to be $1.3 \pm 0.1 \mu$sec.

### F. Three-Parameter ($\alpha$-$\gamma$-Time) Coincidences

It was shown in Ref. 1 that the time spectrum between $Fm^{255}$ $\alpha$ particles and 40- to 100-keV $\gamma$ rays had a half-life of $37 \pm 2$ nsec and had no prompt events. This demonstrates that the 105.73-keV level ($I = \frac{7}{2}, K = \frac{1}{2}$) receives a negligible $\alpha$ population. The present experiment was designed to get some limit for the $\alpha$ intensity to the 105.73-keV level. The procedure was the same as that used by ABP[1] except that we used a three-parameter analyzer and thus obtained the time spectra between various $\alpha$ and $\gamma$-ray gates simultaneously. The $\alpha$ particles were detected with a 6-mm-diam semiconductor detector and the photons were detected with a 2-in.×2-in. NaI(Tl) crystal mounted on an RCA 8575 photomultiplier tube. Fast timing

TABLE VI. Results of two-parameter $\gamma$-$\gamma$ coincidence experiment.

| $\gamma$-ray gate [a] (keV) | $\gamma$ rays [b] (keV) |
|---|---|
| 58.4+60.0 | 58.4, 60.0, 73.0, 81.3, 131.0, and 204.1 |
| 73.0 | 58.4, 60.0, 81.3, 86.0, and 131.0 |
| 81.3 | 60.0, 73.0, 131.0, 132.9, and 204.1 |
| Cf $K_\alpha$ | Cf $K$ x rays, 152.8, 163.8, 177.7, 330.0, 332.0, 366.4, 378.4, and 390.7 |
| 131.0+132.9 | 58.4, 60.0, 73.0, and 81.3 |
| 204.1 | 58.4, 60.0, and 81.3 |
| 332.0 | Cf $K$ x rays |
| 366.3 | Cf $K$ x rays |

[a] Each gate included only the symmetric part of the photopeak and had a width of 6 keV.
[b] The $\gamma$-ray energies are those measured from $\gamma$-singles spectra. The coincidences indicated by underlined $\gamma$ rays are particularly critical in the construction of the decay scheme.

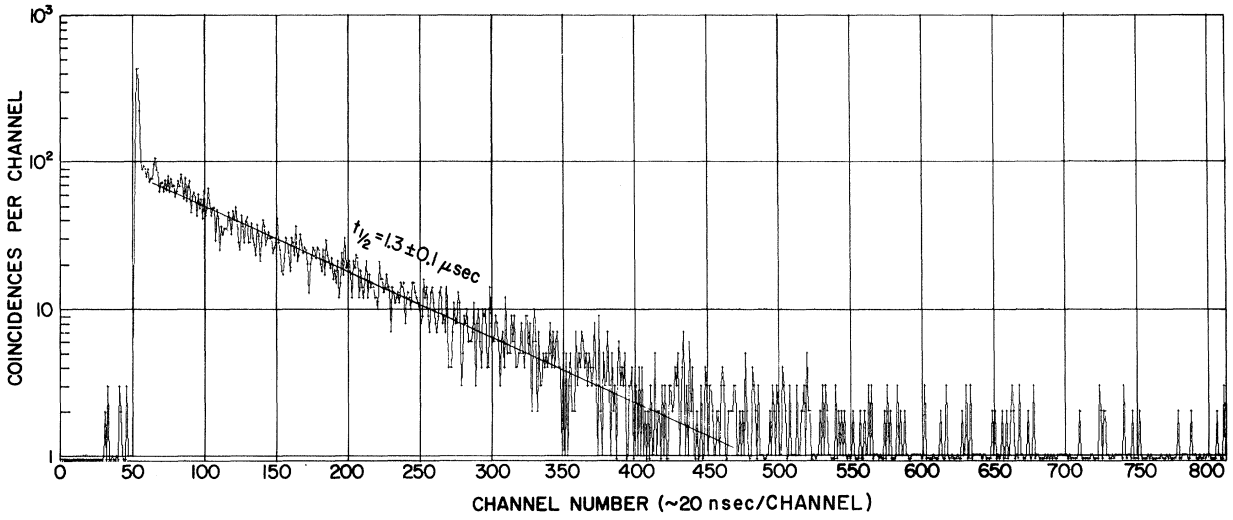


FIG. 9. Time-delay spectrum between 6.59–6.79-MeV $\alpha$ particles and 160–230-keV $\gamma$ rays measuring the decay of the 370.4-keV level.

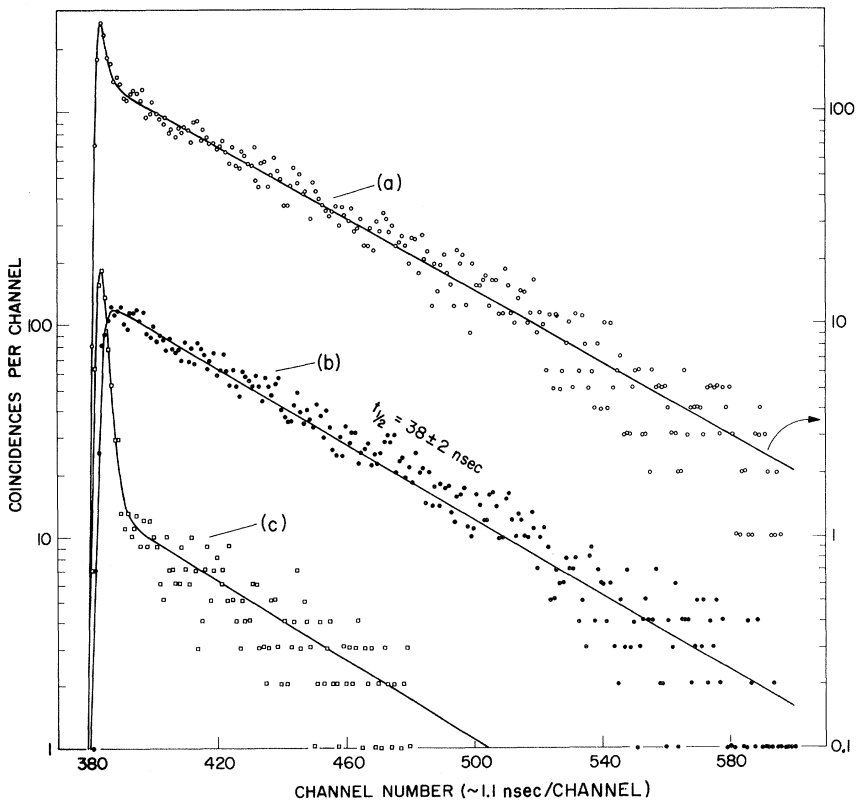


FIG. 10. Time-delay spectrum between $Fm^{255}$ $\alpha$ particles and 40- to 100-keV $\gamma$ rays: (a) the $\alpha$ gate included all $\alpha$ particles above 6.0 MeV; (b) the $\alpha$ gate consisted of the $\alpha_{106}$ peak only (7.01- to 7.03-MeV $\alpha$ particles); and (c) $\alpha$ gate included all $\alpha$ particles between 6.0 and 6.99 MeV. The $\gamma$ gate for each spectrum was the same (40 to 100 keV). The lack of prompt coincidences in (b) indicates that there is very little (<1%) population to the 105.73-keV, $I=\frac{7}{2}$, $K=\frac{1}{2}$ level. Note that spectrum (a) uses the right-hand scale.

pulses were derived with time-pick-off units. Figure 10 shows the time spectra between: (a) all $Fm^{255}$ $\alpha$ particles above 6.0 MeV and 40- to 100-keV $\gamma$ rays; (b) only the $\alpha_{106}$ (no contribution from any other $\alpha$ group) and 40- to 100-keV $\gamma$ rays; and (c) all $\alpha$ particles between 6.0 and 6.99 MeV (to exclude the $\alpha_{106}$ peak) and 40- to 100-keV $\gamma$ rays. From the analysis of these spectra it was found that $\alpha$ intensity to the 105.73-keV level is less than 1%. The best value for the half-life of the 106.3-keV level was found to be $38 \pm 2$ nsec.

The same experimental setup was also used to learn about the time relationship of the $\alpha_{368}$ and $\alpha_{433}$ with 204.1-keV $\gamma$ rays. It was found that the $\alpha_{368}$ and $\alpha_{433}$ groups are not in prompt coincidence with the 204.1-keV $\gamma$ ray. This again establishes that the 370.4-keV level is delayed.

## IV. DISCUSSION

### A. Decay Scheme

The single-particle orbital assignments of the ground state and the 106-keV level of $Cf^{251}$ as $\frac{1}{2}+$ (620↑) and $\frac{7}{2}+$ (613↑), respectively, were made by ABP.[1] The results of our investigation fully support these assignments. In the present work a more precise measurement of the level energies has been made. The excited-state energy, $E_I$, of a rotational member of a band can be calculated from the equation[20]

$$E_I = E_0 + \frac{\hbar^2}{2\mathcal{I}}[I(I+1) + \delta_{K,1/2}\, a(-)^{I+1/2}(I+\tfrac{1}{2})], \qquad (1)$$

where $E_0$ is a constant, $\mathcal{I}$ is the nuclear moment of inertia, and $a$ is the decoupling parameter. The observed level energies for the $K = \frac{1}{2}$ band are in good agreement with the values calculated from Eq. (1) and with values of the rotational constant $\hbar^2/2\mathcal{I}$ and decoupling parameter $a$ as 6.438 and 0.2851 keV, respectively. The measured energies of the members of $K = \frac{7}{2}$ band built on the 106.30-keV level give a value of 6.66 keV for its rotational constant.

From the present measurements, the energy difference between the 105.73-keV, $I = \frac{7}{2}$, $K = \frac{1}{2}$ and the 106.30-keV, $I = \frac{7}{2}$, $K = \frac{7}{2}$ levels is $0.57 \pm 0.02$ keV; the total feed to the $I = \frac{7}{2}$, $K = \frac{1}{2}$ level is $(18 \pm 3)$%; and the half-life of the $I = \frac{7}{2}$, $K = \frac{7}{2}$ state is $38 \pm 2$ nsec, respectively. These values are in good agreement with the corresponding values of $0.56 \pm 0.02$ keV, 16%, and $37 \pm 2$ nsec, respectively, measured by ABP.[1] The calculated[1] $\alpha$ intensity to the $\frac{7}{2}+$ member of the ground-state band, $\frac{1}{2}+$ (620↑), is 0.13% based on the observed $\alpha$ intensities to its lower members and the assumption of pure rotational states. An admixture of the favored band, $\frac{7}{2}+$ (613↑), into this state can augment its $\alpha$ population. The third-order Coriolis mixing[21] of the favored band into the ground-state band proceeds by a $|\Delta K| = 1$ interaction via a $K = \frac{5}{2}$ and a $K = \frac{3}{2}$ band. On the basis of Coriolis interaction calculations, ABP[1] concluded that the $\alpha$ intensity to the $I = \frac{7}{2}$, $K = \frac{1}{2}$ level cannot exceed 0.7%, and the feed (18%) to this level is brought by the 0.57-keV transition. Since we now know the energies of the intermediate $\frac{5}{2}+$ (622↑) and $\frac{3}{2}+$ (622↓) states (544.1 and 177.7 keV, respectively), the calculations were repeated. The calculations gave an $\alpha$ intensity of 0.5% for this state. Thus the detailed analysis of transitions by ABP[1] is still correct. In our experiments we could not detect any $\alpha$ population to the 105.73-keV, $I = \frac{7}{2}$, $K = \frac{1}{2}$ level and place an upper limit of 1% for this $\alpha$ transition.

The rotational bands built on the 177.7- and 544.1-keV levels were first observed by Ahmad[3] and were assigned to the $\frac{3}{2}+$ (622↓) and $\frac{5}{2}+$ (622↑) states, respectively. The present investigation confirms these assignments. The measured $M1$ multipolarity of the 177.7-keV transition restricts the values of $K\pi$ to $\frac{1}{2}+$ and $\frac{3}{2}+$ only. The energies of the band members are in good agreement with the values calculated from Eq. (1) and with a rotational constant of 6.75 keV for a $K = \frac{3}{2}$ band. The 177.7-keV level is also populated by the electron-capture decay of $Es^{251}$ and has been given a $\frac{3}{2}+$ (622↓) state assignment.[4] This assignment is consistent with the $\alpha$-decay hindrance factors to this band (Sec. IV B).

The rotational band built on the 544.1-keV level deexcites mainly to the $\frac{3}{2}+$ (622↓) and $\frac{7}{2}+$ (613↑) bands. The multipolarities of several transitions (332.0, 366.4, and 378.4 keV) populating the 177.7- and 211.6-keV levels have been measured to be $M1$. Thus the only possible values of $K\pi$ for the 544.1-keV level are $\frac{3}{2}+$ and $\frac{5}{2}+$. The spacings of the 544.1-, 590.2-, and 649.1-keV levels give the value of $K$ as $\frac{5}{2}$. The pattern of $\gamma$ rays deexciting this band to lower bands is consistent with a $K\pi = \frac{5}{2}+$ assignment. The measured level energies give the value of the rotational constant as 6.58 keV. This band is given an assignment of $\frac{5}{2}+$ (622↑) neutron hole state. This is the only $\frac{5}{2}+$ state expected to lie in this energy range according to the Nilsson diagram.[2]

It has been shown in Sec. III D that the $\alpha_{368}$ and $\alpha_{433}$ are in coincidence with the 131.0-, 204.1-, and 264.1-keV $\gamma$ rays. From the near equality of the sums of the measured intensities of the two $\alpha$ groups and the measured summed intensities of the 131.0- and 204.1-keV $\gamma$ rays, it is obvious that these transitions are $E1$. This is further substantiated by the upper limit on conversion-electron intensity which is consistent only with an $E1$

multipolarity for these two $\gamma$ rays. It has been established from the $\alpha$-$\gamma$ coincidence experiment that the origin of the 131.0- and 204.1-keV transitions is the 370.4-keV level. The $\gamma$-$\gamma$ coincidence measurements show that the 131.0- and 204.1-keV transitions populate the 239.33- and 166.31-keV levels, respectively. These observations suggest that the only values of $K\pi$ possible for the 370.4-keV state are $\frac{9}{2}-$ and $\frac{11}{2}-$. The half-life of the 370.4-keV level is too long (1.3$\mu$sec) for any known $K$ allowed $E1$ transition in the deformed region.[22] Hence, this state is given an assignment of $\frac{11}{2}-$ (725$\uparrow$) orbital. It should be pointed out that this is the first time this Nilsson state has been observed in any nucleus.

The 434.2-keV level deexcites mainly to the 370.4-keV state. The multipolarity of this transition has been deduced from the intensity of the 63.8-keV $\gamma$ ray and the total $\alpha$ feed to the 434.2-keV level. The $M1$ multipolarity of the 63.8-keV transition thus obtained indicates that the 434.2-keV level is a negative-parity state, and spin values allowed for this state are $\frac{9}{2}$, $\frac{11}{2}$, and $\frac{13}{2}$. As will be shown in the next section, this state cannot be the rotational member of the band built on the 370.4-keV level. Hence, the 434.2-keV state belongs to a new band. The $\gamma$ rays connecting this state to the $\frac{7}{2}+$ (613$\uparrow$) band (268.0- and 328.0-keV $\gamma$ rays) have also been observed. The fact that the intensities of the 268.0- and 328.0-keV transitions compared with that of the 63.8-keV transition are low is not surprising since most $E1$ transitions in the actinide region are found to be retarded.[23] The 434.2-keV level is given an assignment of $\frac{9}{2}-$ (734$\uparrow$) mainly because it is expected to be near this excitation energy. The assignment is consistent with the observed $\alpha$-decay hindrance factor.

### B. $\alpha$ Transition Probabilities

The relative $\alpha$ transition probabilities to the members of a rotational band are functions of the respective vector-addition coefficients and can be calculated semiempirically.[24] As shown in Ref. 1, the observed $\alpha$ intensities to the members of the ground-state band and to the members of the favored band are in good agreement with the intensities calculated from equations in Ref. 24. The relative $\alpha$ abundances to the members of the members of the $\frac{3}{2}+$ (622$\downarrow$) and $\frac{5}{2}+$ (622$\uparrow$) bands have also been found to agree[3] with the calculated values.

The $\alpha$ transition probabilities have also been calculated from Nilsson wave functions by Poggenburg, Mang, and Rasmussen.[25] The calculated intensities have been found to be in reasonable agreement with the experimental values when normalized for the factored $\alpha$ transition. The hindrance factors (which are reciprocal of the reduced $\alpha$ transition probabilities) for the $\frac{11}{2}$ and $\frac{13}{2}$ members of the $\frac{11}{2}-$ (725$\uparrow$) band have been calculated to be $2.2\times10^3$ and $2.6\times10^3$, respectively. The observed hindrance factors of 490 and 130 for the $\alpha_{368}$ and $\alpha_{433}$ transitions, respectively, clearly demonstrate that the 370.4- and 434.2-keV levels do not belong to the same band. It should be pointed out that a fairly strong Coriolis interaction is expected between the $\frac{11}{2}-$ (725$\uparrow$) and $\frac{9}{2}-$ (734$\uparrow$) bands. The somewhat larger intensity (490 compared with Poggenburg's value of $2.2\times10^3$) of the $\alpha_{368}$ group can be attributed to this admixture.

In Sec. IV A, the 434.2-keV level was given an assignment of $\frac{9}{2}-$ (734$\uparrow$) state. No calculations have been carried out for the $\alpha$ population to this state by Poggenburg.[25] However, it has been known from $\alpha$-decay systematics[1,3] that transitions for states involving no change in the intrinsic spin $\sum$ are about an order of magnitude less hindered than those involving a change in the sign of $\sum$. Thus the hindrance factor of 130 seems consistent with the assignment of $\frac{9}{2}-$ (734$\uparrow$) to the 434.2-keV level.

It should be noted that hindrance factors to the members of the $\frac{3}{2}+$ (622$\downarrow$) band are >1000, whereas the hindrance factors to the members of the $\frac{5}{2}+$ (622$\uparrow$) band are between 66 and 150. These $\alpha$-decay hindrance factors are consistent with the assignment of $\frac{3}{2}+$ (622$\downarrow$) Nilsson state to the 177.7-keV level and $\frac{5}{2}+$ (622$\uparrow$) Nilsson state to the 644.1-keV level.

### ACKNOWLEDGMENTS

The authors would like to thank H. Diamond and F. J. Lynch for their help in the analysis of time spectra and A. M. Friedman and R. R. Chasman for helpful discussions.

---

†Based on work performed under the auspices of the U. S. Atomic Energy Commission.

[1]F. Asaro, S. Bjørnholm, and I. Perlman, Phys. Rev. 133, B291 (1964).

[2]S. G. Nilsson, Kgl. Danske Videnskab. Selskab, Mat.-Fys. Medd. 29, No. 16 (1955).

[3]I. Ahmad, Lawrence Radiation Laboratory Report No. UCRL-16888, 1966 (unpublished).

[4]I. Ahmad, R. K. Sjoblom, R. F. Barnes, E. P. Horwitz, and P. R. Fields, Nucl. Phys. A140, 141 (1970).

[5]I. Ahmad, A. M. Friedman, R. F. Barnes, R. K. Sjoblom, J. Milsted, and P. R. Fields, Phys. Rev. 164,

1537 (1967).
[6]F. Asaro and I. Perlman, Phys. Rev. 158, 1073 (1967).
[7]G. R. Choppin, B. G. Harvey, and S. G. Thompson, J. Inorg. Nucl. Chem. 2, 66 (1956).
[8]R. J. Sochacka and S. Siekierski, J. Chromatog. 16, 376 (1964).
[9]J. Milsted, private communication.
[10]J. Milsted, N. Hansen, and A. H. Jaffey, private communication.
[11]M. A. Preston, Phys. Rev. 71, 865 (1947).
[12]J. A. Bearden and A. F. Burr, Rev. Mod. Phys. 39, 125 (1967).
[13]C. M. Lederer, J. M. Hollander, and I. Perlman, *Table of Isotopes* (John Wiley & Sons, Inc., New York, 1967), Appendix III.
[14]Transitions (shells): 23.0 keV ($M_1M_2N_1$); 24.8 keV ($L_3M_1M_2M_3N_1N_2N_3$); 47.8 keV ($L_2L_3M_2M_3N_2N_3O_{2,3}$); 57.9 keV ($L_1L_3$); 58.5 keV ($L_1L_2L_3M_1$); 60.0 keV ($L_1L_2L_3M_1$); 73.0 keV ($L_1M_1$); 81.5 keV ($L_2L_3M_2M_3N_2O_{2,3}$); 133.0 keV ($L_2L_3$).
[15]W. C. Davidon, Argonne National Laboratory Report No. ANL-5990, 1966 (unpublished).
[16]We have similarly derived binding energies from $L$, $M$, and $N$ shells at $Z=95$. Another publication will discuss the problem of transplatonium atomic binding energies more thoroughly.
[17]J. M. Hollander, M. D. Holtz, T. Novakov, and R. L. Graham, Arkiv Fysik 28, 375 (1965).
[18]F. T. Porter, M. S. Freedman, F. Wagner, Jr., and I. S. Sherman, Nucl. Instr. Methods 39, 35 (1966).
[19]R. S. Hager and E. C. Seltzer, Nucl. Data A4, 1 (1968).
[20]A. Bohr and B. R. Mottelson, Kgl. Danske Videnskab. Selskab, Mat.-Fys. Medd. 27, No. 16 (1953).
[21]A. K. Kerman, Kgl. Danske Videnskab. Selskab, Mat.-Fys. Medd. 30, No. 15 (1955).
[22]C. F. Perdrisat, Rev. Mod. Phys. 38, 41 (1966).
[23]F. Asaro, F. S. Stephens, J. M. Hollander, and I. Perlman, Phys. Rev. 117, 492 (1960).
[24]A. Bohr, P. O. Fröman, and B. R. Mottelson, Kgl. Danske Videnskab. Selskab, Mat.-Fys. Medd. 29, No. 10 (1955); P. O. Fröman, Kgl. Danske Videnskab. Selskab, Mat.-Fys. Skrifter 1, No. 3 (1957).
[25]J. K. Poggenburg, H. J. Mang, and J. O. Rasmussen, Phys. Rev. 181, 1697 (1969); J. K. Poggenburg, Lawrence Radiation Laboratory Report No. UCRL-16187, 1965 (unpublished).